SCIENTIFIC REP⚙RTS

OPEN

Interfacial Coupling Effect on Electron Transport in $MoS_2/SrTiO_3$ Heterostructure: An Ab-initio Study

Amreen Bano & N. K. Gaur

A variety of theoretical and experimental works have reported several potential applications of MoS_2 monolayer based heterostructures (HSs) such as light emitting diodes, photodetectors and field effect transistors etc. In the present work, we have theoretically performed as a model case study, MoS_2 monolayer deposited over insulating $SrTiO_3$ (001) to study the band alignment at TiO_2 termination. The interfacial characteristics are found to be highly dependent on the interface termination. With an insulating oxide material, a significant band gap (0.85eV) is found in MoS_2/TiO_2 interface heterostructure (HS). A unique electronic band profile with an indirect band gap (0.67eV) is observed in MoS_2 monolayer when confined in a cubic environment of $SrTiO_3$ (STO). Adsorption analysis showed the chemisorption of MoS_2 on the surface of STO substrate with TiO_2 termination which is justified by the charge density calculations that shows the existence of covalent bonding at the interface. The fabrication of HS of such materials paves the path for developing the unprecedented 2D materials with exciting properties such as semiconducting devices, thermoelectric and optoelectronic applications.

The exfoliation of two-dimensional(2D) graphite commonly known as graphene has opened up a world wide research interest in atomically thin materials over the past decade[1]. A group of such materials in which interlayer interactions are governed by the Van der Waals(vdW) forces includes transition metal dichalcogenides (TMDs) which follows MX_2 structure where M is a transition metal (Mo, W, Re, Nb etc.) and X is a chalcogen (S, Se,Te)[2]. These TMDs offers flexibility in tuning their electronic properties by reducing the number of layers from bulk to monolayer. It gives out from an indirect band gap in 3D systems to a direct semiconducting band gap in 2D monolayer[3,4]. Heterostructures (HSs) comprises of such 2D materials have provided a new realms in device application industry such as light emitting diodes[5], photodetectors[6–8] and field effect transistors[9–11] due to their ability to align band between 2D planes[12–17]. It is relatively quite easy to fabricate a HS with two similer type of structures with lesser lattice mismatch. These heterostructure (HS) includes MoS_2/WS_2[18], $MoS_2/MoSe_2$[19], $MoS_2/SnSe_2$[20], graphene/hBN[21–25], MoS_2/WSe_2[26]. In the present work, we have used STO as a substrate which is an insulator with perovskite structure, widely used for the growth of multiferroics, colossol magneto-resistive manganites, high temperature superconducting cuprates[27]. Recently, a large number of exciting physical properties has been observed in various oxide HSs based on STO substrates such as charge writing[28], resistance switching[29], quasi-2D electron gas (q-2DEG)[30,31], magnetism[32], giant thermoelectric effect[33] and colossal ionic conductivity[34]. These variety of functionalities offers potential applications in oxide electronics[35], thermoelectric materials and solid oxide fuel cells (SOFCs)[36]. In 2004, Ohtomo and Hwang[30] reported a high mobility electron gas at the interface between STO and $LaAlO_3$ HS. Both the oxide materials are band insulators. The conductivity of the interface was found to be STO termination dependent i.e. for TiO_2 terminated STO, the interface was conductive while for SrO termminated STO, it was insulating[31,37–43].

Recently, several experimental investigations have been reported on MoS_2/TiO_2 interface HSs, but no theoretical attempts have been made. Motivated from this, we have studied theoretically the MoS_2/STO HS with an MoS_2/TiO_2 interface using ab-initio approach. We have provided the computational details which are applied to probe several basic features of the electronic structure of MoS_2/TiO_2 interface in Section II. The results on the electronic band structure of HS and isolated sub-systems along with the chemisorption and chemical bonding occuring at the interface near Fermi level (E_f) are reported and discussed in Section III.

Department of Physics, Barkatullah University, Bhopal, 462026, India. Correspondence and requests for materials should be addressed to A.B. (email: banoamreen.7@gmail.com)
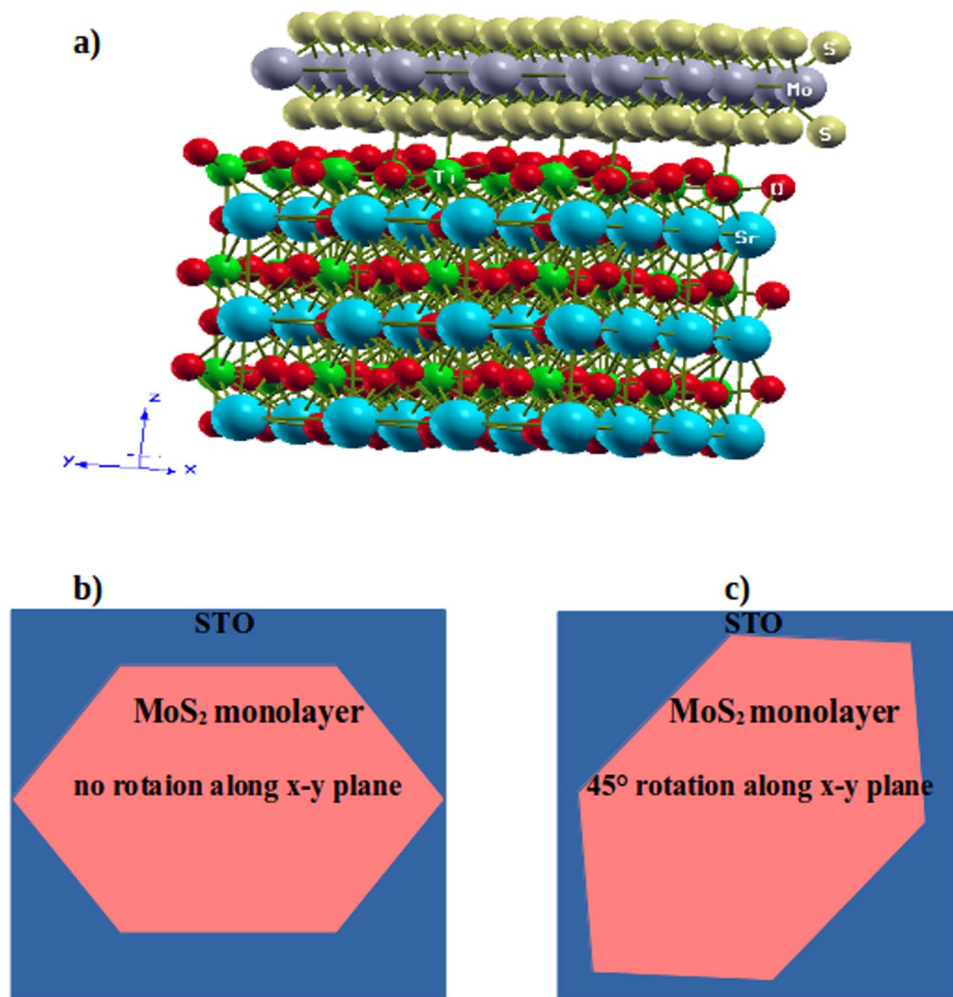
Figure 1. (**a**) Heterostructure of TiO_2 terminated MoS_2/STO; Gray balls indicates Mo atoms, Yellow balls shows S atoms, Blue balls shows Sr atoms, Green balls indicates Ti atoms and Red balls shows O atoms; diagramatic top view of HS showing (**b**) MoS_2 monolayer over STO with no rotation and (**c**) 45° rotation along x-y plane.

Computational Methods

To study the electron transport properties of MoS_2/STO HS, density functional theory (DFT)[44] calculations were carried out by Quantum Espresso Package[45]. The system is analysed by fully relaxing the HS with TiO_2 terminated STO substrate containing supercell of size $2 \times 2 \times 1$ and $4 \times 4 \times 1$ MoS_2 monolayer supercell as shown in Fig. 1(a). Perdew and Zunger functionals[46] within local density approximations (LDA)[47] is used to treat the electronic exchange-interaction. The input parameters, i.e. kinetic energy cutoff and K-mesh are fully optimized before proceeding to the calculations of electronic properties of the HS. Monkhorst-Pack[48] $6 \times 6 \times 1$ K-mesh for Brillouin zone integrations were employed with 544 eV of kinetic energy cutoff. We have taken the value of $U = 4eV$ for effective Coulomb repulsion. All the calculations are based on projector-augmented waves (PAW)[49] method. Generally, the PAW potentials are more accurate than ultrasoft pseudopotentials, because (1) Core radii of PAW potentials are smaller than the radii used for ultrasoft pseudopotentials, (2) PAW potentials reconstruct the exact valence wavefunction with all nodes in the core region. A vaccum of 28 Å is provided normal to the interface in order to present the isolated slab boundary condition. Here, we have chosen a lateral lattice parameters of cubic STO $a_0 = 7.71$ Å, which is optimized for freestanding STO. The lattice mismatch for the interface of HS is found to be 5%, which is expected as the crystal structures of both systems are different i.e. STO is cubic and MoS_2 monolayer is hexagonal. The equilibrium interfacial distance (d_{eq}) between MoS_2 and surface of TiO_2 terminated STO(001) is found to be $d_{eq} = 2.62$ Å. This distance is obtained after relaxing the HS. We have studied the electronic band structures of the HS and $O − 2p$ orbitals are observed at the Fermi level without crossing it with a significant band gap. In this work, we have carried out the spin-polarized calculation and our results indicates that MoS_2/STO HS with TiO_2 termination is nonmagnetic.

Results and Discussion

Electronic band structure. *MoS_2/STO Heterostructure.* We have studied the effect of MoS_2 monolayer on the electronic properties of TiO_2 terminated STO (001). The lattice constant of freestanding STO is 68% larger than that of MoS_2 monolayer which could effect our results of the HS. Hence, we constructed a supercell
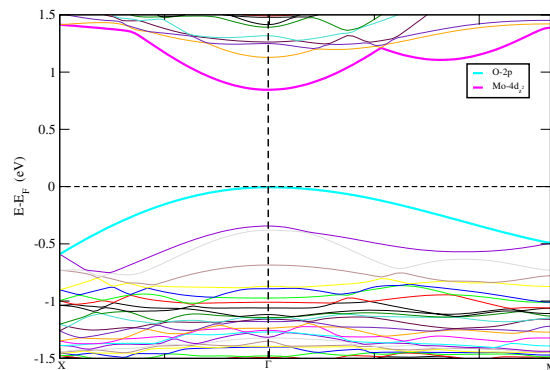
2

Figure 2. Electronic band structure of TiO_2 terminated HS along high symmetry points X(0.5,0,0)-Γ(0,0,0)-M(0.5,0.5,0.0) and the horizontal dashed line implies the E_f set to zero energy at Y-axis.
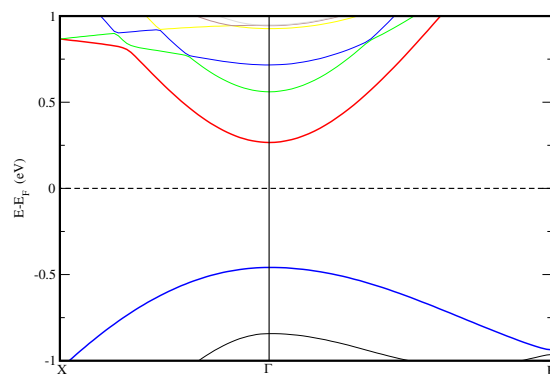

Figure 3. Electronic band structure of STO in TiO_2 termination without MoS_2. Horizontal dashed line implies the E_f set to zero energy at Y-axis.

consisting of a TiO_2 terminated STO containing $2 \times 2 \times 1$ substrate and $4 \times 4 \times 1$ MoS_2 monolayer. The remaining lattice mismatch is only about 5%, which is small enough and it does not effect the electronic structures in the interfaces. The fully relaxed atomic structure of the HS is shown in Fig. 1(a), where clear bonding at the interface can be seen between the two subsystems (STO and MoS_2 monolayer). To make sure that the results we have obtained for the HS are correct, we rotated the MoS_2 monolayer by 45° along x-y plane keeping the STO substrate fixed as shown in Fig. 1(b) and (c) and performed the calculations and found similer results as that of the HS with no rotation of MoS_2 monolayer. To investigate the band alignment of MoS_2/TiO_2 interfaced HS, we have plotted the band structure of the HS. The band diagrams of the sub-systems of the HS are also studied to get a clear insight of the mechanism taking place in the complex HS. The band structure of MoS_2/TiO_2 interface HS is shown in Fig. 2. It can be seen that a band is sitting at the E_f at the valance band maximum (VBM) and energy gap (0.85eV) is visible in TiO_2 terminated HS making it a semiconducting material. The band gap is found to be a direct gap at Γ. The effect of interfacial coupling in this HS gives exciting electronic nature as, an ideal monolayer of MoS_2 is supposed to be a direct band gap material which is found at K high symmetry point while STO in bulk is an indirect band gap (M-Γ)[50] insulating material. Here, when we couple these systems together, it gives out a semiconducting band gap of 0.85eV at Γ. This property brings the HS in the list of potential materials for optoelectronic devices. The conduction band minimum (CBM) is composed of Mo-4d electron states in Fig. 2.

Now we are interested to study the band structure of STO by removing the MoS_2 monolayer. The electronic band structure of STO without MoS_2 monolayer is shown in Fig. 3. We observed from Fig. 3 that when MoS_2 is removed from TiO_2 terminated HS, the VBM shifts down and CBM move towards E_f and reduced band gap (0.72eV). Hence, the effect of MoS_2 monolayer on STO can be analysed as, when MoS_2 monolayer is deposited on STO, a relatively large band gap is obtained and in place of Mo-4d states, now Ti-3d states are seen at CBM. The monolayer is influencing the energies of atoms of STO. Also, we found from Fig. 3 that, the direct band gap is not coming due to the monolayer but STO itself is giving out a direct semiconducting gap at Γ. Therefore, from Fig. 2, we conclude that MoS_2/TiO_2 interface is a semiconductor with a direct narrow energy gap. This indicates the effect of *STO* substrate with TiO_2 termination on the electronic properties of *MOS*$_2$. It shows that *STO* substrate can be used as an ideal substrate for MoS_2-based device applications. Band gaps obtained for other HSs based on MoS_2 are enlisted in Table 1.

Subsystems-STO and MoS$_2$ Monolayer. We have also studied the band structure of STO and MoS_2 monolayer confined within the structural parameters of the STO (001) ($2 \times 2 \times 1$) seperately in order to have a comparative study. We can see in Fig. 4, the ideal cubic STO substrate appears to have a direct band gap (at Γ) of 1.77 eV which

Structures	Reported Band gaps (eV)
MoS_2/WS_2	1.25[54]
Stanene/MoS_2	0.067[55]
MoS_2/SiC	1.34[56]
ZnO/MoS_2	1.48[57]
Graphene/ZnO/MoS_2	1.01[57]

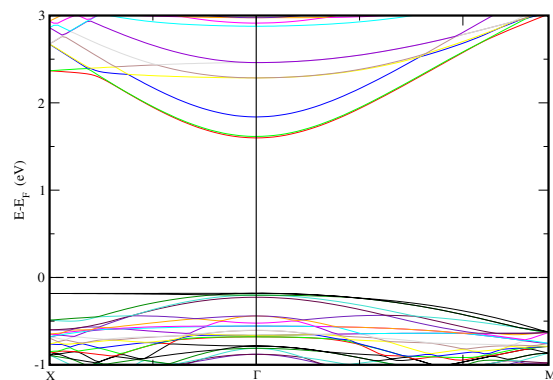**Table 1.** Band gap (E_g) of other heterostructures based on MoS_2.

Figure 4. Electronic band structure of Cubic STO with vacuum along c-axis. High symmetry points are X(0.5,0,0)-Γ(0,0,0)-M(0.5,0.5,0.0) and the horizontal dashed line implies the E_f set to zero energy at Y-axis.
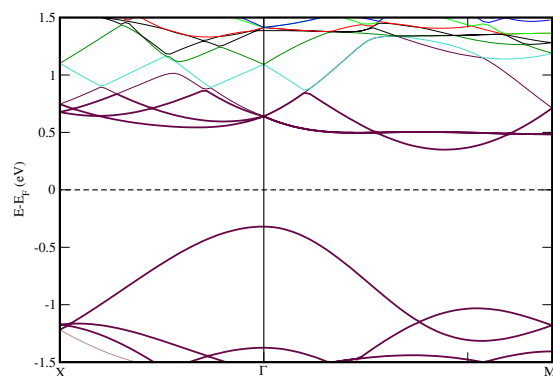

Figure 5. Electronic band structure of MoS_2 Monolayer with cubic confinement. Horizontal dashed line implies the E_f set to zero energy at Y-axis.

is reduced from the bulk STO band gap (3.2eV) arising from p_x, p_y orbitals[51] on the surface layer O ion whose on-site energy is raised by the absence of interations along c-axis. In Fig. 5, the band structure of MoS_2 monolayer is shown. Here, we find an unexpected and unique character of monolayer confined in a cubic unit cell of STO, i.e. it gives out an indirect band gap of 0.67eV. Hence, we can say that the direct band gap of the HS is obtained only due to the contribution of STO with TiO_2 termination. We know that, Silicon is an indirect band gap (1.1 eV) semiconductor (X-L). This reduces its efficiency in electron transport. Hence, we propose a hypothetical view based on our results of monolayer in Fig. 5. If we could fabricate stable freestanding silicon monolayer in honeycomb arrangement as that of ideal MoS_2 monolayer, we may get a direct band gap which is obtained in case of ideal MoS_2 monolayer. An ideal monolayer of MoS_2 gives a direct band gap in honeycomb arrangement, when we confined it in cubic STO dimensions, it becomes an indirect band gap material. In the same way, if the cubic Si could be grown as honeycomb monolayer of MoS_2, it might become a direct band gap system. This hypothesis can be tested by experimental efforts. The E_f of STO alone lies at 0.86 eV whereas for TiO_2 terminated HS, it is found at 1.9893 eV, i.e. E_f of HS lies approximately 1eV above STO valance band maximum (VBM), which nearly at the middle of STO substrate energy gap. Thus, even if strong bonding takes place at the interface, the electronic states at the E_f would deteriorate swiftly into STO layer, this supports the use of thin STO film as substrate[52].

Partial Density of states. The partial density of states (PDoS) further elucidate the electronic band structure. We have displayed the PDoS of TiO_2-terminated HS in Fig. 6. We have observed that the band we saw in
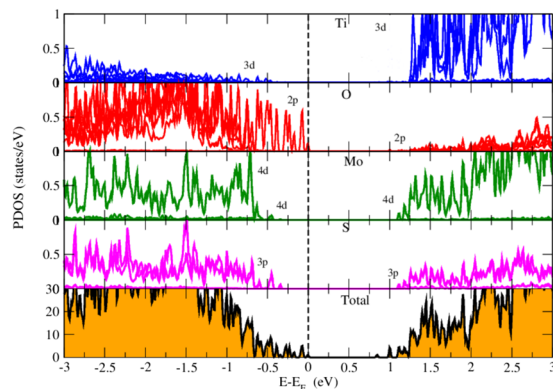
Figure 6. Partial density of states of TiO_2 terminated HS. The E_f is set to zero.
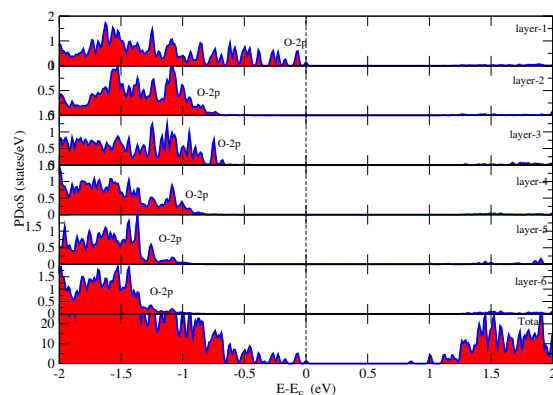

Figure 7. Partial density of states of O atom of each layer in TiO_2 terminated HS. The E_f is set to zero.

Fig. 2, sitting at the E_f is the O-2p states coming from the surface layer of STO. The VBM of HS is composed of O-2p states while CBM is found at 0.85eV with mixed states of Ti-3d, Mo-4d and S-3p. Ti-3d states are present in VB with relatively low intensity PDoS peaks i.e. contribution of Ti in VB is very feeble. Whereas, Mo-4d and S-3p states are clearly seen in both sides of E_f. Also, O-2p states are contributing in VB region actively and are found at E_f but not crossing it. Low intensity peaks of O-2p states are seen is energy below 1.25 eV in CB region.

We studied the contribution of O atoms of each layer of STO to find that O atom of which layer of STO is observed at E_f. Fig. 7 shows the O-2p states of each layer of STO. We begin our analysis from the bottom layer of STO. The common character of O-2p states in each layer is that their contribution in CB is almost negligible. The O-2p states of bottom layer of STO are seen in VB from −1.1eV to far energy range. They are absent near E_f. As we move to the surface layer of STO, the contribution of O-2p states are getting more close to E_f and at the surface layer, O-2p states are found exactly at the E_f but they are not crossing it. These surface O atoms with Mo-4d states of monolayer are giving rise to the existence of energy gap as maximum of VB is composed of O-2p states and minimum of CB is composed of Mo-4d states.

Chemical Bonding. In further calculations, we have investigated the nature of adsorption of MoS_2 on substrate STO, i.e., whether it is chemisorbed or physisorbed. In chemisorption, chemical reaction occurs between the surface of subtrate and the adsorbate (MoS_2) and hence, the new chemical bonds are generated at the interface. Whereas, in case of physisorption, also called as physical adsorption, the electronic properties of the adsorbate are barely perturbed upon adsorption. The bonds can be seen at the interface between the substrate and the adsorbate in Fig. 1(a). This motivates us to investigate the nature of adsorption of the MoS_2 monolayer. In general, vdW interactions exists at the interface of honeycomb like HSs, but in this case, the lattice arrangement is having the cubic STO dimensions hence it is considered that the interactions at the interface will no longer be weak vdW interactions. In order to analyse the nature of adsorption, we randomly shifted the MoS_2 monolayer from the equilibrium distance at the interface d_{eq} where the MoS_2/TiO_2 interface distance is 2.62 Å, upwards upto 5.62 Å and downwards upto 0.3 Å normal to the surface of TiO_2 terminated STO substrate. We have shown the results in Fig. 8. Here we can see two regions I and II. Region I shows the adsorption charateristics of MoS_2 monolayer when the distance from surface of substrate ranges from 2.62 Å to 3.80 Å. We observed an increament in the potential energy of the HS in this region. A deep valley is obtained at d_{eq} which provides the traces of the chemisorption of adsorbate (MoS_2) over surface of TiO_2 terminated STO substrate. As the distance at the interface is further increased, the potential energy starts to fall down. This decreament is recorded in the range from 3.8 Å to 5.62 Å, as we have studied this response in range of distance 0.3 Å, upwards upto 5.62 Å only. As we further
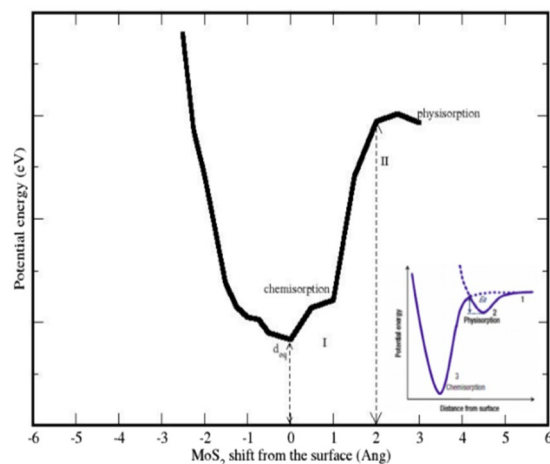
Figure 8. Nature of adsorption of MoS_2 on the surface of STO (001); MoS_2 monolayer is shifted in units of Å. d_{eq} is taken as 0 shift and further shifts are added to d_{eq}; figure in inset shows the ideal adsorption curve shows the trend of chemisorption and physisorption[53].
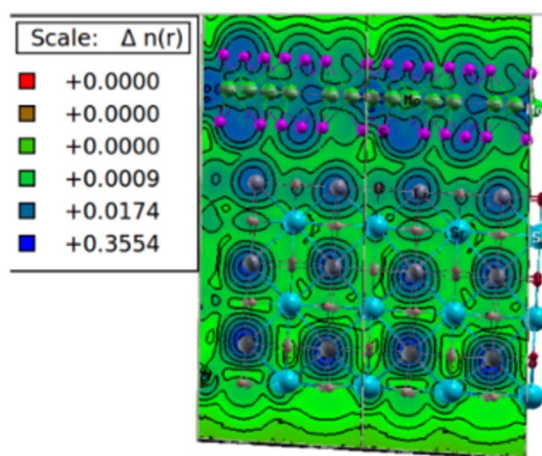

Figure 9. Charge density of TiO_2 terminated HS in (010) plane. The color plate is at right side showing the charge transfer and bonding character at the interface. Atoms are presented as; Blue balls- Sr, Gray balls- Ti, Red balls- O, Magenta balls- S and Green balls- Mo.

decreased the distance lesser than d_{eq}, we can clearly see an abrupt increase in potential energy which indicates the presence of electronic repulsion. If we further decrease this distance, the energy will tend to infinity under the effect of nuclear repulsion. From Fig. 6, we found that the MoS_2/TiO_2 interface is a semiconductor with covalent bonding occuring between Mo-4d and O-2p states. This hybridization of electronic states makes our statement on chemical adsorption more stronger.

The presence of chemisorption of MoS_2 monolayer over STO surface can be justified by inspecting the nature of chemical bonding between the atoms at the interface. To investigate the bonding characteristics between atoms at the interface, we performed the charge density calculations. Charge density provides the information about bonding/repulsion between MoS_2 and STO. Fig. 9 shows the charge density in (010) plane. Maximum values implies the regions where charge increases when MoS_2 and STO coupling takes place. In the substrate STO, we can see the isolated closed spherical isolines around the bottom atoms. These closed isolines indicates the existence of ionic bonding between the atoms of STO at the bottom layer. As we move upwards, ionic bonding is still present till the surface layer of STO. A clear covalent bonding between the surface atoms of STO and MoS_2 monolayer can be seen at the interface. It is considerd that if ionic bonding exists at the interface, the material should be a metal and if there exists an energy gap, it suggest a covalent bond between the atoms. Thus the presence of semiconducting band gap in HS (0.85eV) justifies our results of existance of covalent bonding obtained from adsorption analysis and charge density calculations. This bonding is arising due to the hybridization of O-2p and Mo-4d states in VB region which can be seen from Fig. 7 where the 2p energy states of O and 4d and 3p states of Mo and S atoms respectively are present in the energy range −0.3eV to far VB region. This mixing of states results in the strong covalent bonds between O-2p and Mo-4d states with small contribution of S-3p states.

Conclusion

In summary, we have investigated the electronic band structure and chemical bonding of the MoS_2 monolayer deposited over the STO substrate with TiO_2 termination within the framework of density functional theory. In order to authenticate our results, we have performed all the calculations for the HS with 45° rotated MOS_2 monolayer along x-y plane keeping the substrate fixed. We obtained similar results for such arrangement and hence validates our findings. The interfacial distance (d_{eq}) between MoS_2 and surface of TiO_2 terminated STO(001) is found to be 2.62 Å. The conduction band is mainly composed of Mo-4d and S-3p states along with small contribution of Ti-3d states as well, while valance band is containing O-2p states near E_f which is playing the major roll in the semiconducting nature of the HS. Surface O atoms of STO substrate are found at E_f. A semiconducting band gap is found (0.85eV) and MoS_2 is strongly bonded with the substrate which is seen in the chemical bonding analysis. A unique nature of isolated MOS_2 monolayer confined in STO lattice parameters is observed i.e. it gives an indirect band gap of 0.67eV. This finding can be examined experimentally for application purpose in the case of Si which could be a breakthrough in semiconducting devices. Our adsorption analysis suggests the chemisorption of MoS_2 on surface of STO substrate with TiO_2 termination. MoS_2/TiO_2 terminated HS with a semiconducting band gap offers a potential candidature in thermoelectric and optoelectronic applications.

References

1. Ulstrup, S. *et al.* Spatially resolved electronic properties of single-layer WS_2 on transition metal oxides. *ACS Nano* **10**, 10058–10067 (2016).
2. Lin, Z. *et al.* 2D materials advances: from large scale synthesis and controlled heterostructures to improved characterization techniques, defects and applications. *2D Mater.* **3**, 042001, https://doi.org/10.1088/2053-1583/3/4/042001 (2016).
3. Mak, K. F., Lee, C., Hone, J., Shan, J. & Heinz, T. F. Atomically thin MoS_2: A new direct-gap semiconductor. *Phys. Rev. Lett.* **105**, 136805, https://doi.org/10.1103/PhysRevLett.105.136805 (2010).
4. Liu, H. *et al.* Phosphorene: an unexplored 2D semiconductor with a high hole mobility. *ACS Nano* **8**, 4033–4041 (2014).
5. Cheng, R. *et al.* Electroluminescence and photocurrent generation from atomically sharp WSe_2/MoS_2 heterojunction p-n diodes. *Nano Lett.* **14**, 5590–5597 (2014).
6. Massicotte, M. *et al.* Picosecond photoresponse in van der Waals heterostructures. *Nat. Nanotechnol.* **11**, 42–46 (2016).
7. Yuan, H. *et al.* Polarization-sensitive broadband photodetector using a black phosphorus vertical p-n junction. *Nat. Nanotechnol.* **10**, 707–713 (2015).
8. Wang, X. *et al.* Enhanced rectification, transport property and photocurrent generation of multilayer $ReSe_2/MoS_2$ p–n heterojunctions. *Nano Res.* **9**, 507–516 (2015).
9. Deng, Y. *et al.* Black phosphorus-monolayer MoS_2 van der Waals heterojunction p-n diode. *ACS Nano* **8**, 8292–8299 (2014).
10. Jeong, H. *et al.* Semiconductor-insulator-semiconductor diode consisting of monolayer MoS_2, h-BN, and GaN heterostructure. *ACS Nano* **9**, 10032–10038 (2015).
11. Sun, Q-Q. *et al.* The physics and backward diode behavior of heavily doped single layer MoS_2 based pn junctions. *Appl. Phys. Lett.* **102**, 093104, https://doi.org/10.1063/1.4794802 (2013).
12. Wang, H. *et al.* The role of collective motion in the ultrafast charge transfer in van der Waals heterostructures. *Nat. Commun.* **7**, 11504, https://doi.org/10.1038/ncomms11504 (2016).
13. Huang, C. *et al.* Lateral heterojunctions within monolayer $MoSe_2−WSe_2$ semiconductors. *Nat. Mater.* **13**, 1096–1101 (2014).
14. Wang, F. *et al.* Tunable $GaTe−MoS_2$ van der Waals p-n Junctions with Novel Optoelectronic Performance. *Nano Lett.* **15**, 7558–7566 (2015).
15. Son, Y. *et al.* Observation of switchable photoresponse of a monolayer $WSe_2−MoS_2$ lateral heterostructure via photocurrent spectral atomic force microscopic imaging. *Nano Lett.* **16**, 3571–3577 (2016).
16. Liu, Y. *et al.* Van der Waals heterostructures and devices. *Nat. Rev. Mater.* **1**, 16042, https://doi.org/10.1038/natrevmats.2016.42 (2016).
17. Novoselov, K. S., Mishchenko, A., Carvalho, A. & Castro Neto, A. H. 2D materials and van der Waals heterostructures. *Science* **353**, 9439, https://doi.org/10.1126/science.aac9439 (2016).
18. Tongay, S. *et al.* Tuning interlayer coupling in large-area heterostructures with CVD-grown MoS_2 and WS_2 monolayers. *Nano Lett.* **14**, 3185–3190 (2014).
19. Kang, J., Li, J. B., Li, S. S., Xia, J. B. & Wang, L. W. Electronic structural Moiré pattern effects on $MoS_2/MoSe_2$ 2D heterostructures. *Nano Lett.* **13**, 5485–5490 (2013).
20. Zhou, X. *et al.* Vertical heterostructures based on $SnSe_2/MoS_2$ for high performance photodetectors. *2D Mater.* **4**, 025048, https://doi.org/10.1088/2053-1583/aa6422 (2017).
21. Yankowitz, M. *et al.* Emergence of superlattice Dirac points in graphene on hexagonal boron nitride. *Nat. Phys.* **8**, 382–386 (2012).
22. Ponomarenko, L. A. *et al.* Cloning of Dirac fermions in graphene superlattices. *Nature* **497**, 594–597 (2013).
23. Dean, C. R. *et al.* Hofstadter's butterfly and the fractal quantum Hall effect in moiré superlattices. *Nature* **497**, 598–602 (2013).
24. Hunt, B. *et al.* Massive Dirac fermions and Hofstadter butterfly in a van der Waals heterostructure. *Science* **340**, 1427–1430 (2013).
25. Yu, G. L. *et al.* Hierarchy of Hofstadter states and replica quantum Hall ferromagnetism in graphene superlattices. *Nat. Phys.* **10**, 525–529 (2014).
26. Rivera, P. *et al.* Observation of long-lived interlayer excitons in monolayer $MoSe_2−WSe_2$ heterostructures. *Nat. Commun.* **6**, 6242, https://doi.org/10.1038/ncomms7242 (2015).
27. Chen, Y. *et al.* Metallic and insulating interfaces of amorphous $SrTiO_3$-based oxide heterostructures. *Nano Lett.* **11**, 3774–3778 (2011).
28. Xie, Y. W., Bell, C., Yajima, T., Hikita, Y. & Hwang, H. Y. Charge writing at the $LaAlO_3/SrTiO_3$ surface. *Nano Lett.* **10**, 2588–2591 (2010).
29. Chen, Y. Z., Zhao, J. L., Sun, J. R., Pryds, N. & Shen, B. G. Resistance switching at the interface of $LaAlO_3/SrTiO_3$. *Appl. Phys. Lett.* **97**, 123102, https://doi.org/10.1063/1.3490646 (2010).
30. Ohtomo, A. & Hwang, H. Y. A high-mobility electron gas at the $LaAlO_3/SrTiO_3$ heterointerface. *Nature* **427**, 423–426 (2004).
31. Caviglia, A. D. *et al.* Two-Dimensional Quantum Oscillations of the Conductance at $LaAlO_3/SrTiO_3$ Interfaces. *Phys. Rev. Lett.* **105**, 236802, https://doi.org/10.1103/PhysRevLett.105.236802 (2010).
32. Brinkman, A. *et al.* Magnetic effects at the interface between non-magnetic oxides. *Nat. Mater.* **6**, 493–496 (2007).
33. Ohta, H. *et al.* Giant thermoelectric Seebeck coefficient of a two-dimensional electron gas in $SrTiO_3$. *Nat. Mater.* **6**, 129–134 (2007).
34. García-Barriocanal, J. *et al.* Colossal ionic conductivity at interfaces of epitaxial $ZrO_2:Y_2O_3/SrTiO_3$ heterostructures. *Science* **321**, 676–680 (2008).
35. Mannhart, J. & Schlom, D. G. Oxide interfaces–an opportunity for electronics. *Science* **327**, 1607–1611 (2010).
36. Chambers, S. A. Epitaxial growth and properties of doped transition metal and complex oxide films. *Adv. Mater.* **22**, 219–248 (2010).
37. Ben Shalom, M., Ron, A., Palevski, A. & Dagan, Y. Shubnikov–De Haas oscillations in $SrTiO_3/LaAlO_3$ interface. *Phys. Rev. Lett.* **105**, 206401, https://doi.org/10.1103/PhysRevLett.105.206401 (2010).

38. Xie, Y. W. *et al*. Quantum longitudinal and Hall transport at the *LaAlO₃/SrTiO₃* interface at low electron densities. *Sol. State Commun.* **197**, 25–29 (2014).
39. Fete, A. *et al*. Large modulation of the Shubnikov–de Haas oscillations by the Rashba interaction at the *LaAlO₃/SrTiO₃* interface. *New J. Phys.* **16**, 112002, https://doi.org/10.1088/1367-2630/16/11/112002 (2014).
40. Maniv, E. *et al*. Strong correlations elucidate the electronic structure and phase-diagram of *LaAlO₃/SrTiO₃* interface. *Nat. Commun.* **6**, 8239, https://doi.org/10.1038/ncomms9239 (2015).
41. Yang, M. *et al*. High field magneto-transport in two-dimensional electron gas *LaAlO₃/SrTiO₃*. *Appl. Phys. Lett.* **109**, 122106, https://doi.org/10.1063/1.4963234 (2016).
42. Zeng, S. *et al*. Liquid-gated high mobility and quantum oscillation of the two-dimensional electron gas at an oxide interface. *ACS Nano* **10**, 4532–4537 (2016).
43. McCollam, A. *et al*. Quantum oscillations and subband properties of the two-dimensional electron gas at the *LaAlO₃/SrTiO₃* interface. *APL Mater.* **2**, 022102, https://doi.org/10.1063/1.4863786 (2014).
44. Hohenberg, P. & Kohn, W. Inhomogeneous electron gas. *Phys. Rev.* **136**, B864, https://doi.org/10.1103/PhysRev.136.B864 (1964).
45. Giannozzi, P. *et al*. Quantu Espresso: a modular and open-source software project for quantum simulations of materials. *J.Phys.:Condens.Matter* **21**, 395502, https://doi.org/10.1088/0953-8984/21/39/395502 (2009).
46. Perdew, J. P. & Zunger, A. Self-interaction correction to density-functional approximations for many-electron systems. *Phys. Rev. B* **23**, 5048, https://doi.org/10.1103/PhysRevB.23.5048 (1981).
47. Griffin, S. M. & Spaldin, N. A. A density functional theory study of FeAs comparing LDA+ U, GGA+ U and hybrid functionals. Preprint at https://arxiv.org/abs/1401.2277 (2014).
48. Monkhorst, H. J. & Pack, J. D. Special points for Brillouin-zone integrations. *Phys. Rev. B* **13**, 5188, https://doi.org/10.1103/PhysRevB.13.5188 (1976).
49. Kresse, G. & Joubert, D. From ultrasoft pseudopotentials to the projector augmented-wave method. *Phys. Rev. B* **59**, 1758, https://doi.org/10.1103/PhysRevB.59.1758 (1999).
50. Benrekia, A. R. *et al*. Structural, electronic and optical properties of cubic *SrTiO₃* and *KTaO₃*: Ab initio and GW calculations. *Phys. B* **407**, 2632–2636 (2012).
51. Padilla, J. & Vanderbilt, D. Ab initio study of *SrTiO₃* surfaces. *Surf. Sci.* **418**, 64–70 (1998).
52. Huang, Y. N. & Pickett, W. E. Electronic coupling between a FeSe monolayer film and *SrTiO₃* substrate. *Phys. Rev. B* **95**, 165107, https://doi.org/10.1103/PhysRevB.95.165107 (2017).
53. Khan, M. A., Nadeem, M. A. & Idriss, H. Ferroelectric polarization effect on surface chemistry and photo-catalytic activity: A review. *Surf. Sci. Rep.* **71**, 1–31 (2016).
54. Kosmider, K. & Fernandez-Rossier, J. Electronic properties of the *MoS₂ − WS₂* heterojunction. *Phys. Rev. B* **87**, 075451, https://doi.org/10.1103/PhysRevB.87.075451 (2013).
55. Liang, D. *et al*. Tunable band gaps in *stanene/MoS₂* heterostructures. *J. Mat. Sci.* **52**, 5799–5806 (2017).
56. Min, L., Yu, X. E. & Xi, S. Y. Tunable band gap of *MoS₂−SiC* van der Waals heterostructures under normal strain and an external electric field. *AIP Adv.* **7**, 015116, https://doi.org/10.1063/1.4975399 (2017).
57. Xu, L., Huang, W. Q., Zhou, B. X., Pan, A. & Huang, G. F. Two-dimensional *MoS₂−graphene*-based multilayer van der Waals heterostructures: Enhanced charge transfer and optical absorption, and electric-field tunable dirac point and band gap. *Chem. Mater.* **29**, 5504–5512 (2017).

Author Contributions

A.B. performed all the calculations and prepared the manuscript. N.K.G. provided corrections in the manuscript. Both the authors reviewed the manuscript.

Additional Information

Competing Interests: Financial support has been provided to the author A.B. by Maulana Azad National Fellowship (MANF), ID-48759 of University Grants Commission (UGC), Delhi.

Publisher's note: Springer Nature remains neutral with regard to jurisdictional claims in published maps and institutional affiliations.